J. Fluid Mech. (2001), *vol.* 427, *pp.* 107–129. Printed in the United Kingdom

Evolution of a nonlinear wave field along a tank: experiments and numerical simulations based on the spatial Zakharov equation

By L. SHEMER[1], HAIYING JIAO[1], E. KIT[1] AND Y. AGNON[2]

[1]Department of Fluid Mechanics and Heat Transfer, Faculty of Engineering, Tel-Aviv University, Tel-Aviv 69978, Israel

[2]Department of Civil Engineering, Technion, Haifa 32000, Israel

(Received 20 October 1999 and in revised form 31 July 2000)

Evolution of a nonlinear wave field along a laboratory tank is studied experimentally and numerically. The numerical study is based on the Zakharov nonlinear equation, which is modified to describe slow spatial evolution of unidirectional waves as they move along the tank. Groups with various initial shapes, amplitudes and spectral contents are studied. It is demonstrated that the applied theoretical model, which does not impose any constraints on the spectral width, is capable of describing accurately, both qualitatively and quantitatively, the slow spatial variation of the group envelopes. The theoretical model also describes accurately the variation along the tank of the spectral shapes, including free wave components and the bound waves.

1. Introduction

Shemer *et al.* (1998) studied the evolution of nonlinear wave groups along a laboratory wave tank experimentally, and the results of the measurements were compared with computer simulations based on the cubic Schrödinger equation. This most commonly used nonlinear wave model was originally derived by Zakharov (1968) for infinite water depth. Later, alternative derivations of this equation were presented (see, e.g. Hasimoto & Ono 1972; Yuen & Lake 1975). The cubic Schrödinger equation is accurate to the third-order in wave steepness ε, and describes the envelope evolution of a propagating wave packet with a narrow-frequency bandwidth in deep or intermediate depth water. The study by Shemer *et al.* demonstrated that certain global properties of the spatial wave group evolution could indeed be described by this model equation. The experiments, however, revealed certain subtler features of the evolution process, which could not be adequately described by the cubic Schrödinger equation. In particular, the initially symmetric steep wave group envelopes became skewed as they propagated along the tank. The cubic Schrödinger equation, owing to its symmetric properties, retains the symmetry of the initially symmetric wave group envelope. Thus, the appearance of asymmetric wave groups cannot be described by this model equation.

This failure of the cubic Schrödinger equation prompted Lo & Mei (1985) to apply a modification of this model, the so-called Dysthe equation (1979). In the Dysthe equation, which is valid for deep-water waves and which also describes the evolution of the envelope, an additional nonlinear $O(\varepsilon^1)$ term appears which accounts for the spectral width. Application of this equation by Lo & Mei gave agreement with experimental observations.

It should be noticed that both the cubic Schrödinger and the Dysthe equations can be derived from the Zakharov (1968) equation by applying appropriate limits on the spectral width (Zakharov 1968; Stiassnie 1984). For this reason, it can be expected that the numerical calculations based on the Zakharov equation, which is free of any constraints on the spectral width, can be advantageous for predictions of the evolution of nonlinear wave fields. This conjecture was suggested by several authors (Yuen & Lake 1982; Lo & Mei 1985; Trulsen & Dysthe 1997), although it remained unconfirmed. The Zakharov equation (Zakharov 1968; Yuen & Lake 1982) is indeed the most general nonlinear wave model, which describes temporal evolution of deep nonlinear waves in Fourier space. The modulation of each wave component is due to nonlinear near resonant interaction of four waves (the so-called Class I interactions). Zakharov's derivation is based on the Hamiltonian formalism. It is accurate to the third order in wave steepness, and has no restrictions on the spectral width. Stiassnie & Shemer (1984) extended the derivation to intermediate depth and to the next order, to account for the so-called Class II (five waves) near-resonant interactions. Krasitskii (1990, 1994) and Glozman, Agnon & Stiassnie (1993) extended the original derivation of Zakharov. The original (sometimes called 'reduced') Zakharov equation is considerably simpler than its recent modifications. Its accuracy in predicting the domains of instability of nonlinear Stokes waves was demonstrated by Stiassnie & Shemer (1984). They compared the results based on the 'reduced' Zakharov equation with the exact potential flow computations by Longuet-Higgins (1978), McLean *et al.* (1981) and McLean (1982). Quantitative agreement between these two computations was obtained up to Stokes wave steepness exceeding 0.3. Shrira, Badulin & Kharif (1996) applied the Zakharov equation to explain the appearance of the crescent patterns on the sea surface, which were first observed by Su (1982). Their analysis was based on an extension of the earlier study of Class II interactions by Stiassnie & Shemer (1987) by modifying the Zakharov equation to account for weakly non-conservative effects.

Shemer & Chamesse (1999) performed detailed experiments on Benjamin–Feir instability of gravity–capillary waves (Benjamin & Feir 1967) and compared the results with computations based on the Zakharov equation. These computations predicted certain qualitative and quantitative variation in the shape of the instability domains with the carrier wave frequency and amplitude. Those effects were indeed observed in the experiments. The Benjamin–Feir linear stability analysis, however, can only provide an indication of wave evolution on a short timescale.

The Zakharov equation is generally accepted as a superior model for the description of the evolution of nonlinear water waves. In spite of that, no comparison of computations based on this model with experiments on the long-time properties of an evolving system of waves in a wave tank under controlled conditions has yet been performed.

In any comparison of computations based on the Zakharov equation with the experiments in a wave tank, the following considerations have to be taken into account. First, the Zakharov integral equation represents a continuous model. In contrast to that, in the laboratory experiments, periodic signals with finite periods are usually used to drive the wavemaker, and the Fourier transform of these signals results in a discrete spectrum. In other words, in order to use the Zakharov model, it must be properly discretized. This problem has already been settled by Rasmussen & Stiassnie (1999), in which a basic form of two-dimensional discretized Zakharov equation is presented.

The second difficulty is that the standard form of the Zakharov equation describes

slow temporal variation of the surface elevation distributed in an infinite space domain, in which time t is treated as the slow variable with the initial condition at $t = 0$. In contrast to that, in the laboratory tank, a wavemaker is customarily set at one end of the wave tank and the desired temporal variation of the surface elevation is generated by this wavemaker. Care is usually taken to eliminate wave reflection from the far end of the tank. Thus, the wave tank can be treated as semi-infinite with the known initial condition at $x = 0$. The wave gauges are located at fixed measuring points along the tank. The experimentally obtained results describe the unidirectional slow spatial variation of the surface elevation distributed in the time domain, in which distance x is treated as the slow variable. Modification of the governing equation is therefore required in order to describe slow spatial evolution of a wave field in a fixed coordinate system. A unidirectional version of such an equation is developed and presented in this study. In the current simulations, the development of the amplitude of each frequency component in the spectrum of the wave field is followed along the tank. The contributions of the free components, as well as of the related second-order and third-order bound components to the instantaneous surface elevation and the amplitude spectrum are calculated separately. In this sense, the restriction mentioned in Melville & Rapp (1988), that Zakharov's model is restricted to obtaining solutions for the evolution of the envelope of the first harmonic band, is removed. A quadratic model for such evolution on variable depth was derived by Agnon & Sheremet (1997) and Agnon (1999). The evolution of a wave envelope in shallow water in a tank was studied experimentally as well as numerically by the application of the Korteweg–de Vries equation by Kit *et al.* (2000).

In this paper, the evolution of a wave field with a given initial frequency spectrum along the tank is studied both experimentally and by applying the spatial Zakharov model. A unidirectional version of this model is developed in the present study. A more general derivation based on the Hamiltonian formulation is currently being carried out by Zakharov (personal communication). The simplest possible initial wave spectra are considered. A monochromatic wavetrain cannot be expected to develop meaningful interaction along the finite length of the tank. The next possible simplest spectral shape is a bimodal spectrum, i.e. the superposition of two waves with different frequencies and identical amplitudes. The surface elevation due to these initial conditions can be seen as a product of a sinusoidal envelope slowly varying in time and a faster sinusoidal carrier wave. The next initial spectral shape considered here has three dominant modes. In the time domain, the resulting surface elevation is very similar to the first case. The last considered initial spectrum has a Gaussian shape and thus includes numerous harmonics. The shape of the envelope in this case is Gaussian as well. Similar initial conditions were applied in Shemer *et al.* (1998).

2. Basic equations

The third-order Zakharov integral equation, which describes slow temporal evolution of gravity waves in inviscid fluid of constant (infinite or finite) depth can be expressed as:

$$\mathrm{i}\frac{\partial B(\boldsymbol{k},t)}{\partial t} = \iiint_{-\infty}^{\infty} T_{0,1,2,3}\, B^*(\boldsymbol{k}_1,t)B(\boldsymbol{k}_2,t)B(\boldsymbol{k}_3,t) \times \delta(\boldsymbol{k}+\boldsymbol{k}_1-\boldsymbol{k}_2-\boldsymbol{k}_3)\exp\left(\mathrm{i}(\omega+\omega_1-\omega_2-\omega_3)t\right)\mathrm{d}\boldsymbol{k}_1\,\mathrm{d}\boldsymbol{k}_2\,\mathrm{d}\boldsymbol{k}_3, \quad (1)$$

where * denotes complex conjugate. The kernel $T_{0,1,2,3}$ is given in Stiassnie & Shemer (1984). The subscript j stands for the arguments of the kernel, k_j, with 0 standing for

no argument. The argument of the exponential function may become close to zero under the constraints imposed by the Dirac δ-function. This fact is distinguished by the definition of a nearly resonating quartet:

$$\boldsymbol{k} + \boldsymbol{k}_1 - \boldsymbol{k}_2 - \boldsymbol{k}_3 = 0, \quad |\omega + \omega_1 - \omega_2 - \omega_3| \leqslant O(\varepsilon^2). \tag{2}$$

Equation (1) represents the mathematical model for describing the slow temporal evolution of the free Fourier components for Class I, or quartet, nearly resonating interactions.

The dependent variable $B(\boldsymbol{k}, t)$ in (1), which represents the free components in the wave field, is related to a generalized complex 'amplitude' $b(\boldsymbol{k}, t)$. This complex amplitude is composed of the horizontal Fourier transform of the surface elevation $\hat{\eta}(\boldsymbol{k}, t)$ and of the velocity potential at the free surface $\hat{\phi}^s(\boldsymbol{k}, t)$:

$$b(\boldsymbol{k}, t) = [\varepsilon B(\boldsymbol{k}, t_2) + \varepsilon^2 B'(\boldsymbol{k}, t, t_2) + \varepsilon^3 B''(\boldsymbol{k}, t, t_2) \ldots] \exp(-\mathrm{i}\omega(\boldsymbol{k})t) \tag{3}$$

$$b(\boldsymbol{k}, t) = \left(\frac{g}{2\omega(\boldsymbol{k})}\right)^{1/2} \hat{\eta}(\boldsymbol{k}, t) + \mathrm{i}\left(\frac{\omega(\boldsymbol{k})}{2g}\right)^{1/2} \hat{\phi}^s(\boldsymbol{k}, t), \tag{4}$$

where ε is a small parameter representing the magnitude of nonlinearity, and the slow timescale is defined as $t_2 = \varepsilon^2 t$. Equation (3) implies that the wave field can be decomposed into a dominant, slowly varying in time component B, and small but rapid bound components $B', B'', \ldots$. The corresponding bound components of the wave field, $B', B'', \ldots$, which do not obey the linear dispersion relationship, can be expressed in terms of B. The second-order and the third-order bound components B' and B'', as well as the kernels necessary for their computations are given in Stiassnie & Shemer (1984, 1987).

In the present experiments, waves generated by a wavemaker, which is driven by a periodic computer-generated signal, propagate along the tank. Equation (1), therefore, has to be modified to describe unidirectional spatial evolution of a wave system generated at the wavemaker ($x = 0$).

Thus, the waves are periodic in time, with period T, and frequencies

$$\omega_{n_0} = 2n_0\pi/T \quad (n_0 = 1, 2, \ldots). \tag{5}$$

Some of the ideas used in the derivation of the nonlinear Schrödinger equation (Zakharov 1968; Stiassnie & Shemer 1984) are used here. In that derivation, the frequency spectrum was assumed to be confined to a narrow band around a carrier wavenumber k. Here, we split the spectrum into a superposition of a number of such narrow bands, each of them centred about one of the discrete set of wavenumbers k_{n_0}. The surface elevation is then written as a sum of travelling waves with slowly varying amplitudes. In the present application, the waves are strictly periodic in time. Hence, the envelope is a function of x only, and not of t. In general, a partial differential equation in slow space and time can be derived, of which the traditional (temporal) Zakharov equation, and the new (spatial) Zakharov equation, are both special instances (Zakharov, personal communication 1999). These two special equations are convenient when initial conditions are prescribed in time and in space, respectively.

Since $b(k, t)$ is periodic in time, applying (3) we may define:

$$C_{n_0}(k) = \frac{1}{T}\int_0^T \mathrm{d}t\, B(k, t_2) \exp(-\mathrm{i}(\omega(k) - \omega_{n_0})t). \tag{6}$$

Conversely,

$$B(k,t_2)=\sum_{n_0=1}^{\infty}C_{n_0}(k)\exp\left(\mathrm{i}(\omega(k)-\omega_{n_0})t\right). \tag{7}$$

C_{n_0} corresponds closely to A in § 3.2 of Stiassnie & Shemer (1984), where a narrow spectrum is assumed, and a single A (slowly varying in time) is used to derive the nonlinear Schrödinger equation.

The Fourier transform of C_{n_0} with respect to $k-k_{n_0}$, scaled by $(2\omega_{n_0}/g)^{1/2}$ is denoted by $A_{n_0}(x)$. The set $\{A_{n_0}(x), n_0=1,2,3,\ldots\}$ is the frequency spectrum at x.

$$A_{n_0}(x)=\left(\frac{2\omega_{n_0}}{g}\right)^{1/2}\frac{1}{2\pi}\int_{-\infty}^{\infty}C_{n_0}(k)\exp\left(\mathrm{i}(k-k_{n_0})x\right)\mathrm{d}k. \tag{8}$$

The amplitudes of the waves, a_{n_0}, are related to the surface elevation, η, through

$$\eta(x,t)=Re\sum_{n=1}^{\infty}A_{n_0}(x)\exp\left(\mathrm{i}(k_{n_0}x-\omega_{n_0}t)\right), \tag{9}$$

where

$$\omega_{n_0}^2=gk_{n_0}\tanh k_{n_0}h \tag{10}$$

h being the water depth. This is similar to the relation of η to the variable $B(k,t)$ in the Zakharov equation (1), valid to leading order:

$$\eta(x,t)=\frac{1}{2\pi}\int_{-\infty}^{\infty}\left(\frac{\omega(k)}{2g}\right)^{1/2}\left\{B(k,t)\exp\left(\mathrm{i}(kx-\omega t)\right)+\text{c.c.}\right\}\mathrm{d}k \tag{11}$$

where c.c. is the complex conjugate.

We shall now derive the spatial Zakharov equation for the slow evolution of $A_{n_0}(x)$. Using (7), the left-hand side of (1) is written as:

$$\mathrm{i}B_t=-\sum_{n_0=1}^{\infty}(\omega(k)-\omega_{n_0})\,C_{n_0}(k)\exp\left(\mathrm{i}(\omega(k)-\omega_{n_0})t\right). \tag{12}$$

$\omega-\omega_{n_0}$ can be expanded in a Taylor series:

$$\omega-\omega_{n_0}=c_{g_{n_0}}(k-k_{n_0})+\text{h.o.t.}$$

where $c_{g_{n_0}}=\dfrac{\partial\omega_{n_0}}{\partial k_{n_0}}$ is the group velocity and h.o.t. are higher-order terms. Thus,

$$\mathrm{i}B_t=-\sum_{n_{0=1}}^{\infty}c_{g_{n_0}}(k-k_{n_0})C_{n_0}(k)\exp\left(\mathrm{i}(\omega(k)-\omega_{n_0})t\right). \tag{13}$$

The right-hand side of (1) is written in terms of C_{n_0} as follows

$$\iiint_{-\infty}^{\infty}\mathrm{d}k_1\,\mathrm{d}k_2\,\mathrm{d}k_3\;\; T_{0,1,2,3}\sum_{n_1=1}^{\infty}\sum_{n_2=1}^{\infty}\sum_{n_3=1}^{\infty}C_{n_1}^{*}(k_1)C_{n_2}(k_2)C_{n_3}(k_3)$$
$$\times\exp\left(-\mathrm{i}(\omega+\omega_{n_1}-\omega_{n_2}-\omega_{n_3})t\right)\delta(k+k_1-k_2-k_3). \tag{14}$$

We divide both sides of (13) and (14) by $\mathrm{e}^{-\mathrm{i}\omega t}$ and take the Fourier transform with respect to time. This amounts to collecting terms with equal time dependence. We then multiply by $(2\omega_{n_0}/g)^{1/2}$ and take the inverse Fourier transform (with respect to

$k - k_{n_0}$). The result is

$$\begin{aligned} \mathrm{i}c_{g_{n_0}} a_{n_{0_x}} = \frac{1}{2\pi}\left(\frac{2\omega_n}{g}\right)^{1/2} \iiint_{-\infty}^{\infty} \mathrm{d}k_1\, \mathrm{d}k_2\, \mathrm{d}k_3\; T_{0,1,2,3} \\ \times \sum_{n_1=1}^{\infty}\sum_{n_2=1}^{\infty}\sum_{n_3=1}^{\infty} C^*_{n_1}(k_1) C_{n_2}(k_2) C_{n_3}(k_3) \\ \times \exp\left(\mathrm{i}(k_2 + k_3 - k_1 - k_{n_0})x\right) \delta(\omega_{n_0} + \omega_{n_1} - \omega_{n_2} - \omega_{n_3}). \end{aligned} \tag{15}$$

Since the significant interaction is near resonance, we expand $T_{0,1,2,3}$ in a Taylor series about T_{n_0,n_1,n_2,n_3}:

$$T_{0,1,2,3} = T_{n_0,n_1,n_2,n_3} + O(\Delta k), \tag{16}$$

where Δk is the width of the narrow spectral band around each wavenumber. We approximate the former kernel by the latter, and identify the inverse Fourier transforms of $C^*_{n_1}, C_{n_2}$ and C_{n_3} with respect to $(k - k_1), (k - k_2)$ and $(k - k_3)$ in the right-hand side of (15). Substituting the approximation of $T_{0,1,2,3}$ by T_{n_0,n_1,n_2,n_3} into (15) gives

$$\begin{aligned} \mathrm{i}c_{g_{n_0}} A_{n_{0_x}} = \sum_{n_1=1}^{\infty}\sum_{n_2=1}^{\infty}\sum_{n_3=1}^{\infty} 2\pi^2 \left(\frac{\omega_n g^2}{\omega_{n_1}\omega_{n_2}\omega_{n_3}}\right)^{1/2} T_{n_0,n_1,n_2,n_3} \\ \times A^*_{n_1} A_{n_2} A_{n_3} \exp\left(-\mathrm{i}(k_{n_0} + k_{n_1} - k_{n_2} - k_{n_3})x\right) \\ \times \delta(\omega_{n_0} + \omega_{n_1} - \omega_{n_2} - \omega_{n_3}). \end{aligned} \tag{17}$$

Note that the integrand of the spatial version of the Zakharov equation (17) is non-zero only for near resonant quartets $(k_{n_0}, k_{n_1}, k_{n_2}, k_{n_3})$, so that $k_{n_0} + k_{n_1} - k_{n_2} - k_{n_3} = O(\varepsilon^2)$.

The terms which are $O(k_j - k_{n_j})$ give rise to terms of the order of $A^*_{j_x}, A_2, A_3$ (which are of higher order), as well as terms which are proportional to the horizontal velocity of the mean flow, as discussed by Stiassnie & Shemer (1984). Thus, the model equation (17) (which is valid for spectra of any width) is formally of the same order as the modified nonlinear Schrödinger equation due to Dysthe (1979), which was derived for a narrow spectrum. The parameter ε used in the nonlinear Schrödinger equation model to describe the spectral width (as well as the wave steepness) corresponds here to the spectral resolution. The spatial Zakharov equation can be extended to a quasi three-dimensional setting, as well as to include Class II nonlinear interaction terms, which are $O(\varepsilon^4)$.

The initial conditions must be calculated according to the initial amplitude and the initial phase of each initial input free component at $x = 0$.

3. Description of the experiment

The experiments are performed in a wave tank, which is 18 m long and 1.2 m wide, with transparent sidewalls and windows at the bottom. The tank is filled to a mean water depth of 0.60 m. Waves are generated by a 'Seawave Simulation' RSW 30-60 wavemaker system. This modular type wavemaker, which consists of four independent paddle sections hinged near the bottom of the tank, is located at one end of the tank. In these experiments, all four paddles operate in phase with identical amplitude. The wavemaker is driven by a computer-generated signal. In order to perform measurements for various water depths, a false bottom made of marine plywood plates has been constructed in the tank. In order to reduce the wave reflection from the end of the tank, a sloping energy-absorbing beach is installed at

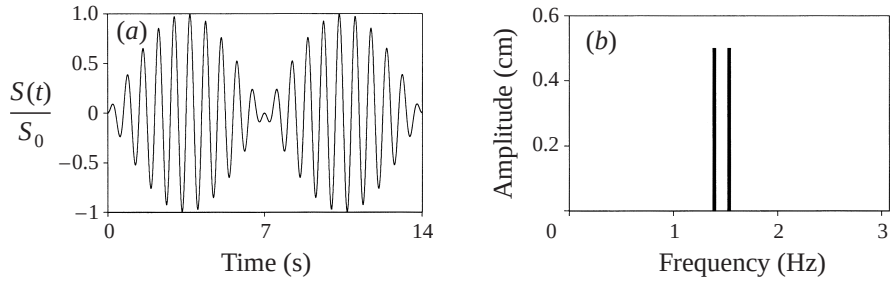

FIGURE 1. Wavemaker displacement and its spectrum for the driving signal (18).

the far end of the tank. Experiments are carried out for two constant water depths: 60 cm and 17 cm.

The instantaneous surface elevation is measured by a set of four resistance wave gauges. The wave gauge wires are made of 0.3 mm stainless steel. The sensors are supported by bars mounted on a carriage, which can be moved along the tank. Measurements of the surface elevation are performed at eight carriage locations along the central line of the tank. The spacing between the adjacent gauges on the bar is about 0.4 m, the distance between the measuring stations being about 1.6 m. Information on the variation of the instantaneous surface elevation with time is thus obtained for 32 locations x from the wavemaker, which covers the range of distances from the wavemaker $0.24\,\mathrm{m} \leqslant x \leqslant 11.31\,\mathrm{m}$.

Three kinds of driving signals with two carrier wave periods, $T_1 = 0.7\,\mathrm{s}$ and $T_2 = 0.9\,\mathrm{s}$ are employed in the experiments. Each driving signal is repeated periodically and controlled by the computer.

The first driving signal is given by:

$$s(t) = s_0 \cos(\Omega t) \cos(\omega_0 t) \quad (\Omega = \omega_0/20), \tag{18}$$

where s_0 is the forcing amplitude, ω_0 is the radian carrier frequency, and Ω is the modulation frequency. The period of this forcing signal is $\tau = 20T_0$, T_0 being the carrier wave period $T_0 = 2\pi/\omega_0$. The spectrum of this signal is bimodal with two distinct peaks of identical amplitude shifted from the carrier frequency ω_0 by $\pm\omega_0/20$. The wavemaker displacement during one driving signal period and its amplitude spectrum ($T_0 = 0.7\,\mathrm{s}$) are presented in figure 1.

The second driving signal is given by:

$$s(t) = s_0 |\cos(\Omega t)| \cos(\omega_0 t) \quad (\Omega = \omega_0/20). \tag{19}$$

The envelope of this signal is identical to that given by (18), but the period of the forcing signal in this case is $\tau = 10T_0$. Its spectrum has a maximum peak at the carrier frequency ω_0 and consists of a set of discrete frequencies spaced by $\omega_0/10$, with only the two closest to the carrier frequency sidebands being significant. The wavemaker displacement during one driving signal period and the amplitude spectrum of this driving signal ($T_0 = 0.7\,\mathrm{s}$) are presented in figures 2(a) and 2(b) respectively.

In the third series of experiments, the driving signal is defined as:

$$s(t) = s_0 \exp(t/mT_0)^2 \cos(\omega_0 t) \quad (m = 3.5, \quad -16T_0 < t < 16T_0). \tag{20}$$

It is repeated periodically with the period $\tau = 32T_0$ and generates wave groups that are widely separated. The discrete frequency spectrum of (20) has a Gaussian shape with the maximum peak at ω_0 and a larger number of significant peaks. The

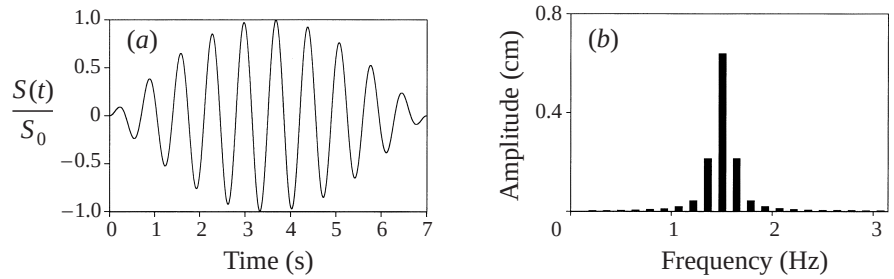

FIGURE 2. Wavemaker displacement and its spectrum for the driving signal (19).

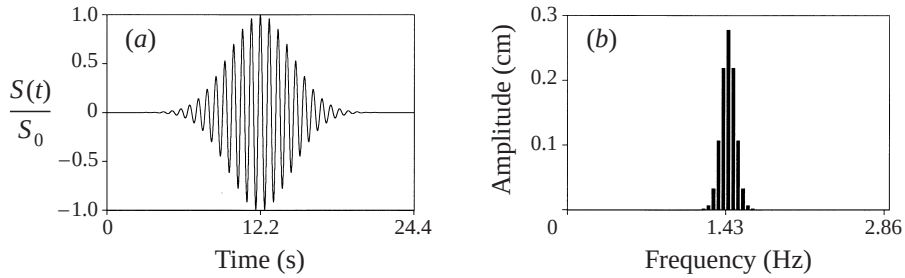

FIGURE 3. Wavemaker displacement and its spectrum for the driving signal (20).

longer period of the forcing signal results in a finer spectral resolution of $\omega_0/32$. The corresponding graphs are presented in figure 3.

The maximum driving amplitudes s_0 for each shape of the driving signal are selected so that close to the wavemaker, the resulting carrier wave has the maximum wave amplitudes a_0 corresponding to the wave steepness $\varepsilon = k_0 a_0$ required in each particular experimental run.

4. Results

4.1. *Selection of the initial conditions and number of free modes considered*

In the system of discretized equations (17), each equation determines the spatial evolution along the tank of a given free wave. In order to apply this system for studying the evolution of the nonlinear wave field in the tank, the number of these free waves considered (and thus the number of ODEs solved) has to be determined.

As mentioned by Shemer & Stiassnie (1985) and Stiassnie & Shemer (1987), at least three free waves are required in order to enable significant nonlinear interaction, i.e. a change in the wave amplitudes. This holds for both Class I and Class II interactions. A long time evolution pattern with only three free waves was studied in Stiassnie & Shemer (1987) for Class I interactions, in which the considered three free waves included one finite-amplitude carrier wave and two initially weak most unstable disturbances obtained by linear stability analysis. No additional free waves were incorporated in their model of the evolution.

The spectra of the driving signals considered in the present study, however, include two harmonics of identical amplitude for the driving signal (18) and, strictly speaking, an infinite number of harmonics for the driving signals (19) and (20). All adopted periodic driving signals have a narrow spacing between the adjacent modes, $f/f_0 \ll 1$. Additional free modes can be generated in the course of the evolution process owing

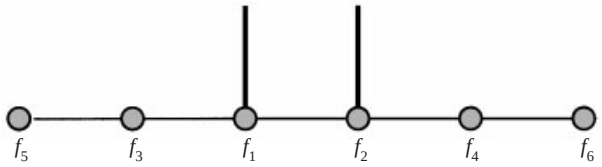

FIGURE 4. Model with 6 free components.

to nonlinear interactions. A sketch showing the four additional closest free waves that can be generated for the driving signal (18) is presented in figure 4.

At the wavemaker, there are only two free modes f_1 and f_2 with finite amplitudes, the amplitudes of all the other modes are set to be zero. Nonlinear interactions among the two main free modes and their neighbours result in the gradual appearance along the tank of additional free modes, such as f_3 and f_4, and then remote free modes f_5 and f_6. Additional, even more remote sideband-free components can be added if necessary. Similar procedures can be applied for the driving signals (19) and (20).

It can thus be expected that the wave spectrum becomes wider in the process of evolution along the tank. The desired number of modes for each specific case has to be determined from practical considerations. In the present study, the initial number of free modes is determined based on the initial wave spectrum and the wave steepness. The system of equations (17) is solved numerically, and the resulting wave spectra are analysed along the tank. In the following runs, the number of free modes can be either increased or decreased, depending on the obtained simulated spectra. The number of free waves is considered to be adequate when the simulated amplitudes at both ends of the frequency spectrum are sufficiently small for the whole extent of the wave tank. This means that there are no effective nonlinear interactions between the modes in the adopted spectrum and more remote modes.

Once the number of the desired free modes n_0 is determined, the corresponding resonating terms must be selected and calculated. For each free mode considered, there are four kinds of combination that satisfy the near resonant condition. These combinations include each free mode taken four times, which interacts with itself, then each possible pair of two free modes, each taken twice. Both these types of combination satisfy exact resonance conditions. In addition, there are combinations of three free modes, in which one of the waves is taken twice, and combinations of four different modes. For those types of combination, the resonant conditions are only approximately satisfied.

All terms based on those four types of combination for each free wave are selected by computer. The symmetry of the interaction coefficient with respect to the last two indices, $T_{j,k,m,n} = T_{j,k,n,m}$ allows the number of independent terms to be decreased. After the number of free modes is chosen and the resonating sets are selected, the Zakharov equation is expressed as a set of mode-coupled nonlinear complex ordinary differential equations (ODEs).

The evolution of the free waves $A(f_n, x), n = 1, \ldots, N$, along the tank is computed by solving a set of mode-coupled N nonlinear complex ODEs, together with the specified initial conditions by using the fourth-order Runge–Kutta method. The exact form of each equation constituting this system is given in the Appendix.

Once the problem of the evolution of the free components is solved, the related second-order and third-order bound components can be computed according to the discretized equations given in the appendix of Stiassnie & Shemer (1987). The corre-

Number of bound wave n	Wavenumber k_n	Wave frequency χ_n	Amplitude A'
$n_0 + n_0(j-1) + k$	$k_j + k_k$	$-\omega_j - \omega_k$	$-V^{(1)}_{n,j,k} A_j A_k / (\omega_n - \omega_j - \omega_k)$
$n_0 + n_0^2 + n_0(j-1) + k$	$-k_j + k_k$	$\omega_j - \omega_k$	$-V^{(2)}_{n,j,k} A_j^* A_k / (\omega_n + \omega_j - \omega_k)$
$n_0 + 2n_0^2 + n_0(j-1) + k$	$-k_j - k_k$	$\omega_j + \omega_k$	$-V^{(3)}_{n,j,k} A_j^* A_k^* / (\omega_n + \omega_j + \omega_k)$

TABLE 1. The second-order bound components.

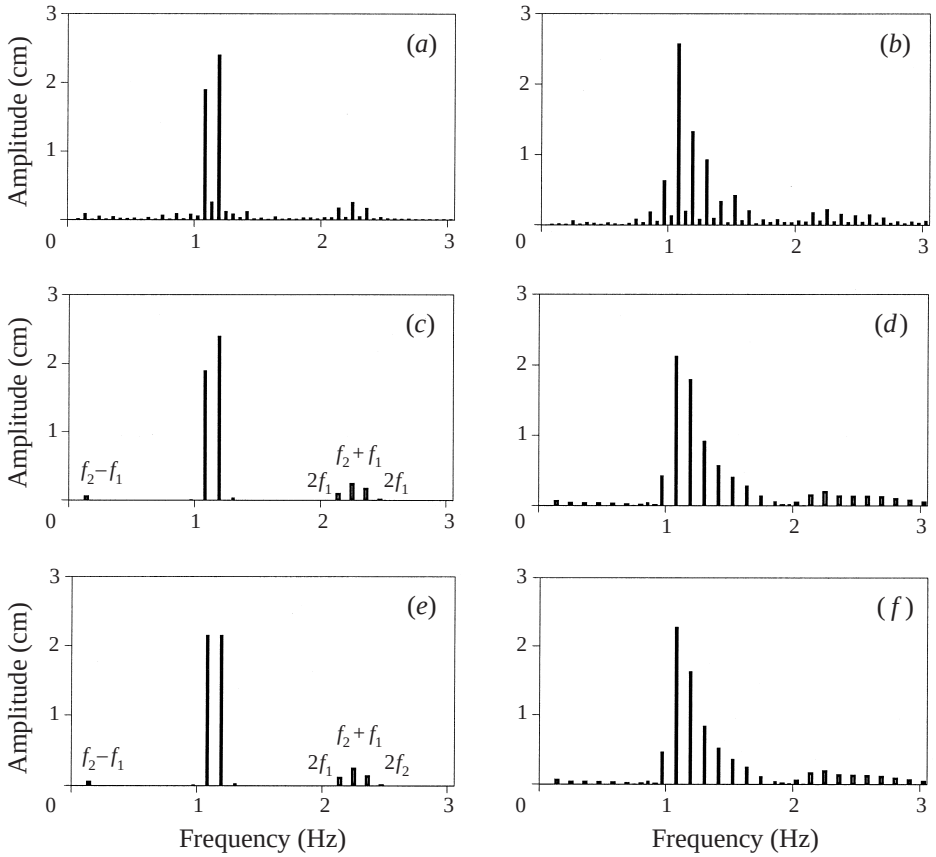

FIGURE 5. Effect of the initial conditions, driving signal (18), $h = 0.6\,\mathrm{m}$, $T_0 = 0.9\,\mathrm{s}$, $\varepsilon = 0.21$. Measured at (*a*) $x = 0.24\,\mathrm{m}$ and (*b*) $x = 9.47\,\mathrm{m}$ amplitude spectra. Simulated amplitude spectra (*d*, *f*) at $x = 9.47\,\mathrm{m}$ for (*a*) asymmetric and (*b*) symmetric initial conditions at $x = 0$.

sponding wavenumbers and wave frequencies of the second-order bound components A' are given in table 1.

If n_0 is the number of the free waves, the total number of the second-order bound components $n_2 = 3n_0^2$, and of the third-order bound components $n_3 = 4n_0^3$. The accumulated effect of the third-order bound components A'' proved to be vanishingly small, even for the highest forcing amplitudes employed in this study (Jiao 1999). These components thus can be disregarded in the following results, saving considerable computer time without any noticeable effect on the accuracy.

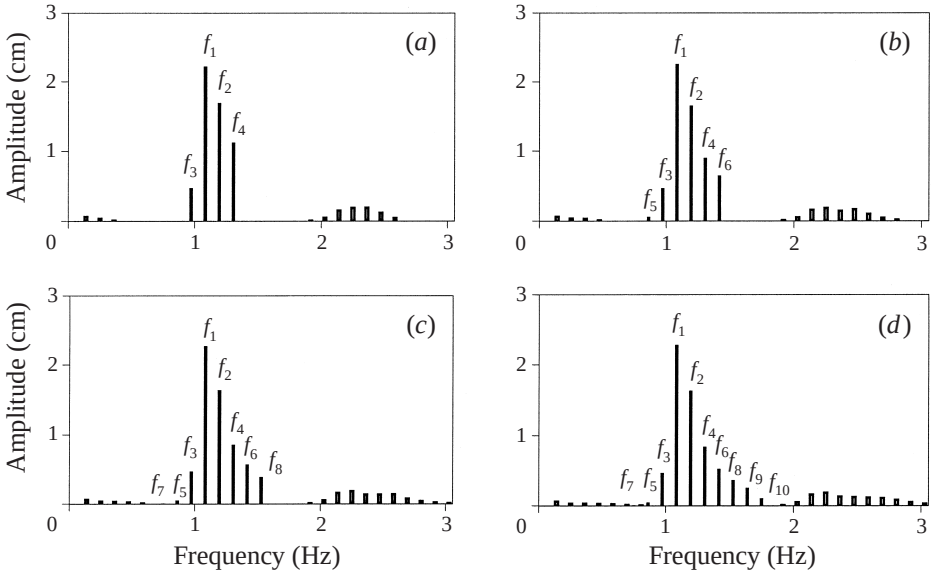

FIGURE 6. Effect of the number of free modes. Simulation results at $x = 9.47$, initial conditions as in figure 5(*e*). (*a*) 4 free modes; (*b*) 6 free modes; (*c*) 8 free modes; (*d*) 10 free modes.

With all free and second-order bound wave components known, the total surface elevation η can be obtained as:

$$\eta = \frac{1}{2\pi} \sum_{n=1}^{n_0+3n_0^2} \left(\frac{\omega_n}{2g}\right)^{1/2} [\tilde{A}_n \exp(\mathrm{i}(k_n x + \chi_n t)) + \text{c.c.}]. \tag{21}$$

For free waves, $\tilde{A}_n$ are calculated for each mode with wavenumber k_n and wave frequency $\chi_n = -\omega_n$. For bound waves, $\tilde{A}_n, k_n$ and χ_n are calculated according to table 1.

Owing to imperfections, the spectral content of surface elevation variation in the vicinity of the wavemaker is somewhat different from that of the driving signal and varies slightly from one experimental run to another. An example of the surface elevation spectrum measured in the tank in the close vicinity of the wavemaker ($x = 0.24$ m) is given in figure 5(*a*). In this example, the driving signal (18) with carrier wave period $T_0 = 0.9$ s is applied at the water depth $h = 0.6$ m ($k_0 h = 3.0$) for the high-amplitude case, $\varepsilon = 0.21$. The corresponding spectrum measured at a remote location ($x = 9.47$ m) is presented in figure 5(*b*). The spectrum presented in figure 5(*a*) is characterized by two dominant peaks of slightly unequal amplitudes of about 2 cm each and several lesser peaks with amplitudes smaller than 0.25 cm. The frequency resolution of the experimentally obtained spectra is $2\Delta f = (f_2 - f_1)/2$, in agreement with the period of the driving signal (18). Minor peaks are observed in figures 5(*a*) and 5(*b*) at the carrier wave frequency $f_0 = (f_2 + f_1)/2$, as well as at frequencies separated from f_0 by integer multiples of $2\Delta f$. Comparison of figures 5(*a*) and 5(*b*) indicates that those peaks remain of minor importance along the tank. Introduction of these harmonics into the initial condition in a number of numerical simulations resulted in a similar behaviour, and those peaks remained small throughout the whole process of the spatial evolution. These experimental and numerical results therefore

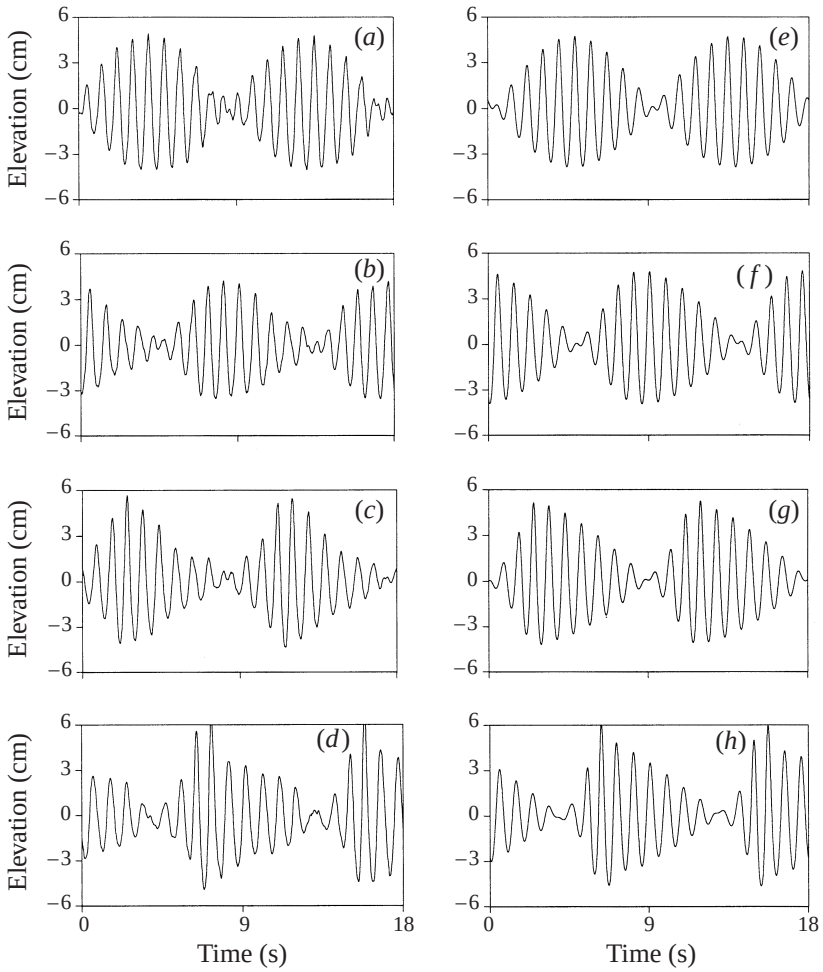

FIGURE 7. Measured (left-hand column) and simulated using 12 free modes (right-hand column) surface elevation. Wave group parameters as in figure 5. (a, e) $x = 0.24$ m, (b, f) $x = 3.69$ m, (c, g) $x = 6.58$ m, (d, h) $x = 9.47$ m.

provide justification for reducing the spectral resolution of computations with the driving signal (18) by disregarding those harmonics.

Two possible initial conditions at $x = 0$ in the numerical simulations can thus be considered. In the first, the initial spectral shape corresponding to the dominant peaks measured in the tank is selected (figure 5*c*). The second option is the initial condition corresponding to that of the driving signal with two equal peaks (figure 5*e*). The height of those peaks is taken as corresponding to the mean energy of the two harmonics (f_1 and f_2) in figure 5(*a*). The additional three high harmonic peaks and one low harmonic peak in figure 5(*a*) are related to the two dominant peaks and therefore can be seen as the corresponding bound components. These bound components can be computed from the given values of the free waves f_1 and f_2 using the expressions from table 1. These bound components are also plotted in figures 5(*c*) and 5(*f*). It should be noted that in contrast to the model simulations, the free and bound components could not be separated in experimental observations. The

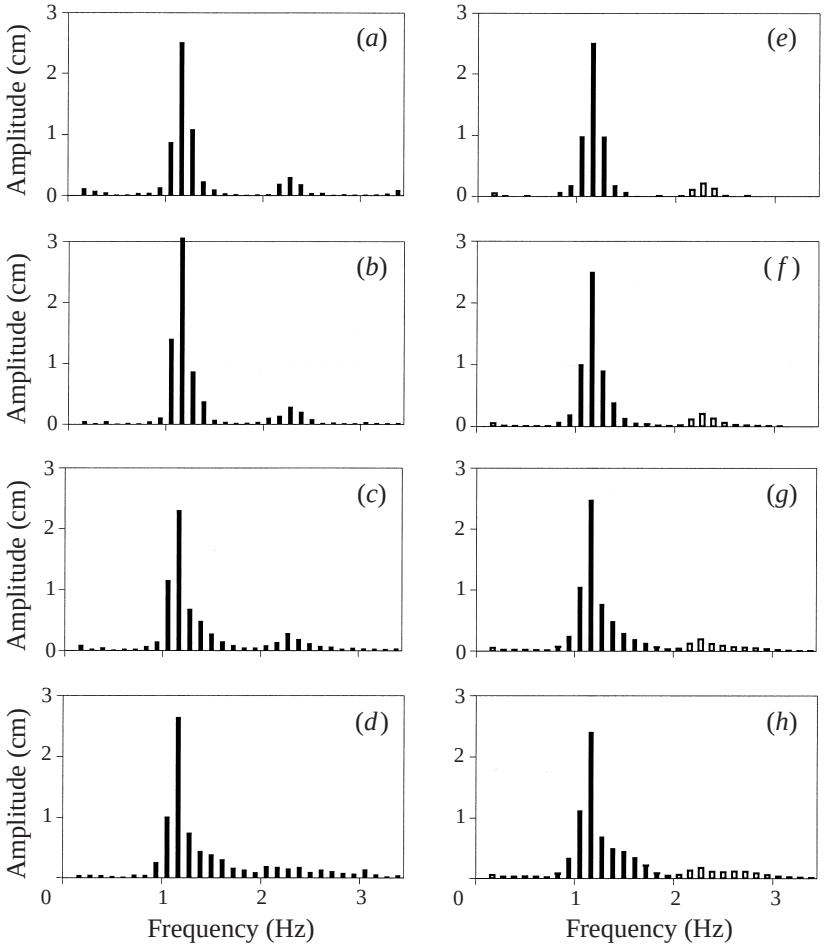

FIGURE 8. Measured (left-hand column) and simulated using 12 free modes (right-hand column) amplitude spectra. Driving signal (19), $h = 0.6$ m, $T_0 = 0.9$ s, $\varepsilon = 0.21$. Locations as in figure 7.

simulated bound components are distinguished in the presented figures from the free components.

The comparison of the simulated spectra at a remote location (figure 5*d*, *f*) with the experimental results (figure 5*b*) shows that the agreement in the case of two equal peaks is at least as good as in the alternative case. Thus, in the following Zakharov model simulations, the simpler driving signal shapes (18)–(20) and their corresponding spectra are chosen as the initial conditions.

All simulations presented in figure 5 were performed using 12 free modes. This number of free modes was selected using the procedure described above, which requires vanishing free mode amplitudes at the edges of the spectrum. The effect of the number of free modes for the conditions of figure 5 is illustrated in figure 6. The results presented in figure 6(*a*) show that when only 4 free modes are incorporated in the evolution process, the simulated amplitude spectrum is totally different from that of the experimentally measured (figure 5*b*). The amplitudes of the two extreme free components, f_3 and f_4, are quite large and their possible interactions with other free modes leading to higher and lower harmonics are effectively cut off. With the number

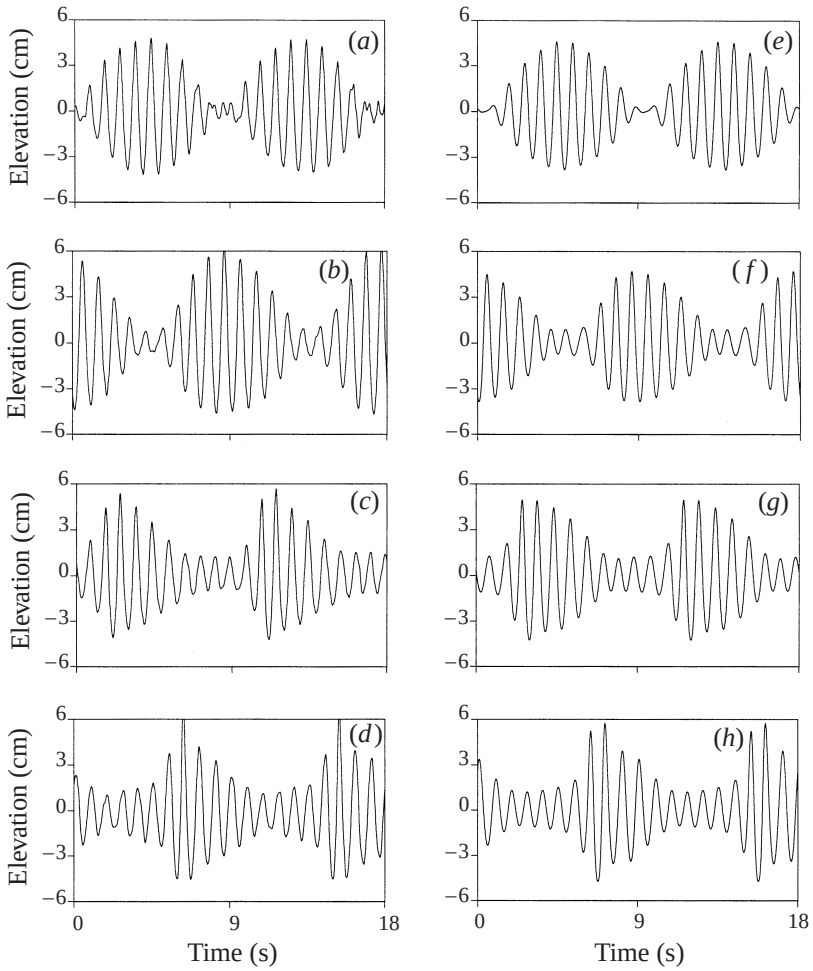

FIGURE 9. Measured and simulated surface elevations for conditions and locations of figure 8.

of free modes increased to 6 (figure 6*b*), and then further increased to 8 (figure 6*c*) and to 10 (figure 6*d*), the simulated results are gradually approaching those obtained in the experiments. At the same time, the amplitudes of the two extreme free components decrease as expected. In figure 6(*d*), the amplitude of the low-frequency extreme free component f_7 is already quite small. Therefore, there is no need for additional free modes at this end of the spectrum, while more free modes, f_{11} or f_{12}, are still required at the high-frequency end, since the amplitude of the free component f_{10} in figure 6(*d*) is not sufficiently small. When the number of free modes is increased to 12 (figure 5*f*), the simulated spectrum is close to the measured one and the amplitudes at both ends of the spectrum of free components are quite small. Thus, in this particular case, there is no further need to increase the required number of free modes.

4.2. *Detailed comparison of experiments and numerical simulations*

Since no interesting evolution patterns were observed for the small-amplitude cases, only results for the intermediate and the large amplitudes are presented here. In what follows, each of figures 7–15, which present the simulated surface elevations and the amplitude spectra, consists of eight frames. The left-hand column (*a–d*) represents the

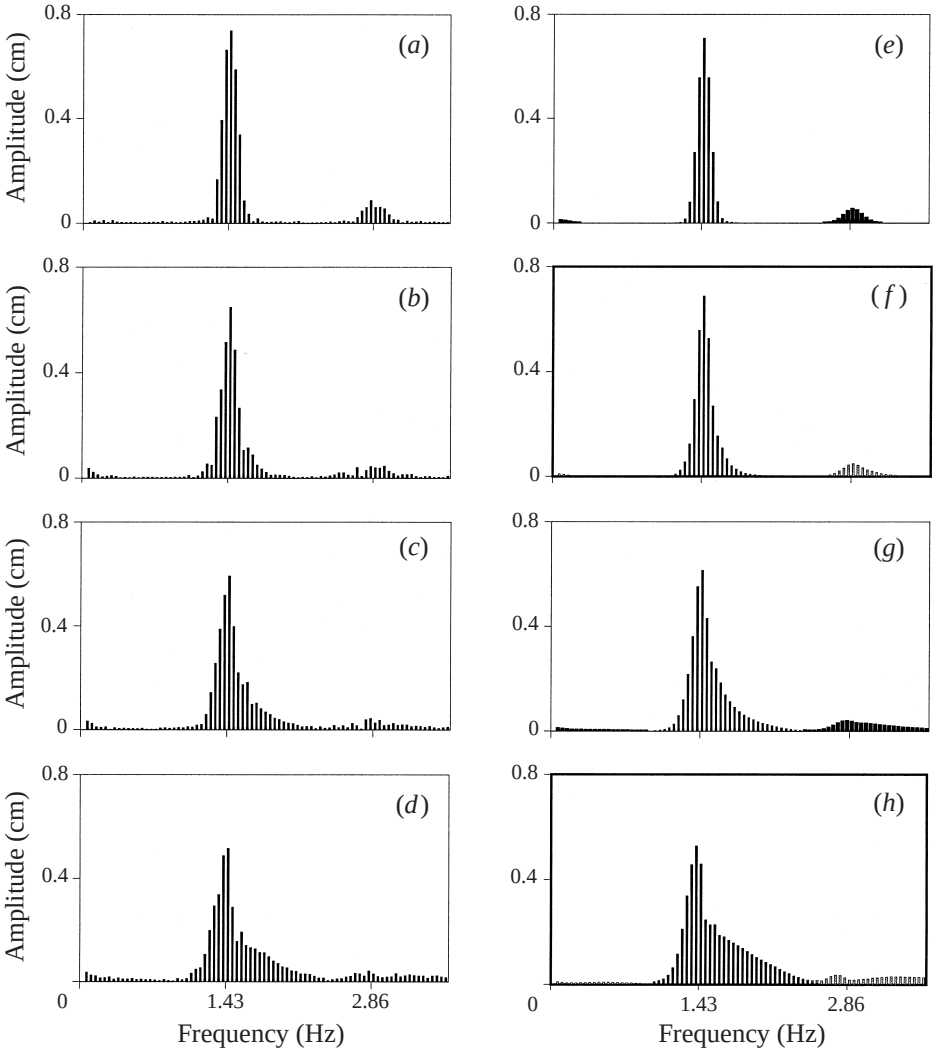

FIGURE 10. Measured (left-hand column) and simulated using 39 free modes (right-hand column) surface elevations. Driving signal (20), $h = 0.6\,\mathrm{m}$, $T_0 = 0.7\,\mathrm{s}$, $\varepsilon = 0.21$. (a, e) $x = 0.24\,\mathrm{m}$, (b, f) $x = 2.89\,\mathrm{m}$, (c, g) $x = 5.78\,\mathrm{m}$, (d, h) $x = 8.67\,\mathrm{m}$.

measured variations of the surface elevation with time in the vicinity of the wavemaker ($x = 0.24\,\mathrm{cm}$), and at the remote locations typically around $x = 3.0\,\mathrm{m}$, $x = 6.0\,\mathrm{m}$, and $x = 9.0\,\mathrm{m}$, or the experimentally determined amplitude spectra calculated at the corresponding locations. The right-hand column (*e–h*) represents the corresponding numerically simulated results at the same locations as in the experiments.

The temporal variation of the surface elevation for the conditions of figure 5 is presented in figure 7. This figure demonstrates that the simulations reflect properly not only the modification of the amplitude spectrum along the tank, but also the evolution of the group shape. Gradual development along the tank of the envelope asymmetries, both left–right and trough–crest, can be seen clearly in the experimental results as well as in the simulations. Similar left–right asymmetry, which is manifested

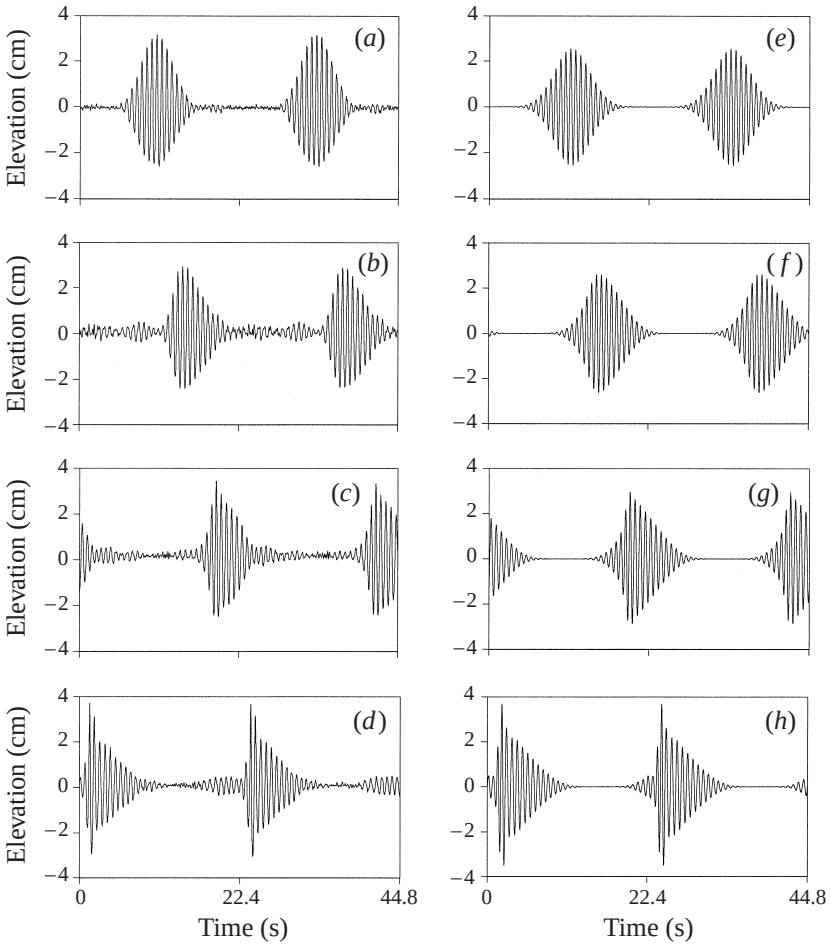

FIGURE 11. Measured and simulated surface elevations for conditions and locations of figure 10.

in the forward leaning of the wave group front, was reported by Lo & Mei (1985) for an initial bimodal spectrum resembling that employed here.

The results presented in figure 8 for the amplitude spectra and in figure 9 for the temporal variation of the surface elevation are for the case with $h = 0.6\,\mathrm{m}$, $T_0 = 0.9\,\mathrm{s}$, ($k_0 h = 3.0$), driving signal (19) and $\varepsilon = 0.21$. The results are given at the same locations as in figure 7. In these frames, both the simulated results and the experimental observations demonstrate similar energy spreading in the course of the propagation of waves away from the wavemaker. This spreading can be observed both in the amplitude spectra and in the surface elevation, which becomes especially prominent at the fourth location ($x = 9.47\,\mathrm{m}$).

Next, results obtained for the driving signal shape given by (20) with the same wave steepness $\varepsilon = 0.21$ are presented in figure 10 for the amplitude spectra and in figure 11 for the surface elevation. In those figures, the carrier wave period $T_0 = 0.7\,\mathrm{s}$ and the water depth $h = 0.6\,\mathrm{m}$ ($k_0 h = 4.93$). The qualitative and even quantitative agreement between the simulations and the experimental results in this case, which includes numerous free modes up to $n_0 = 36$, is as impressive as in the previous cases with simpler initial spectral shapes. The above results clearly demonstrate

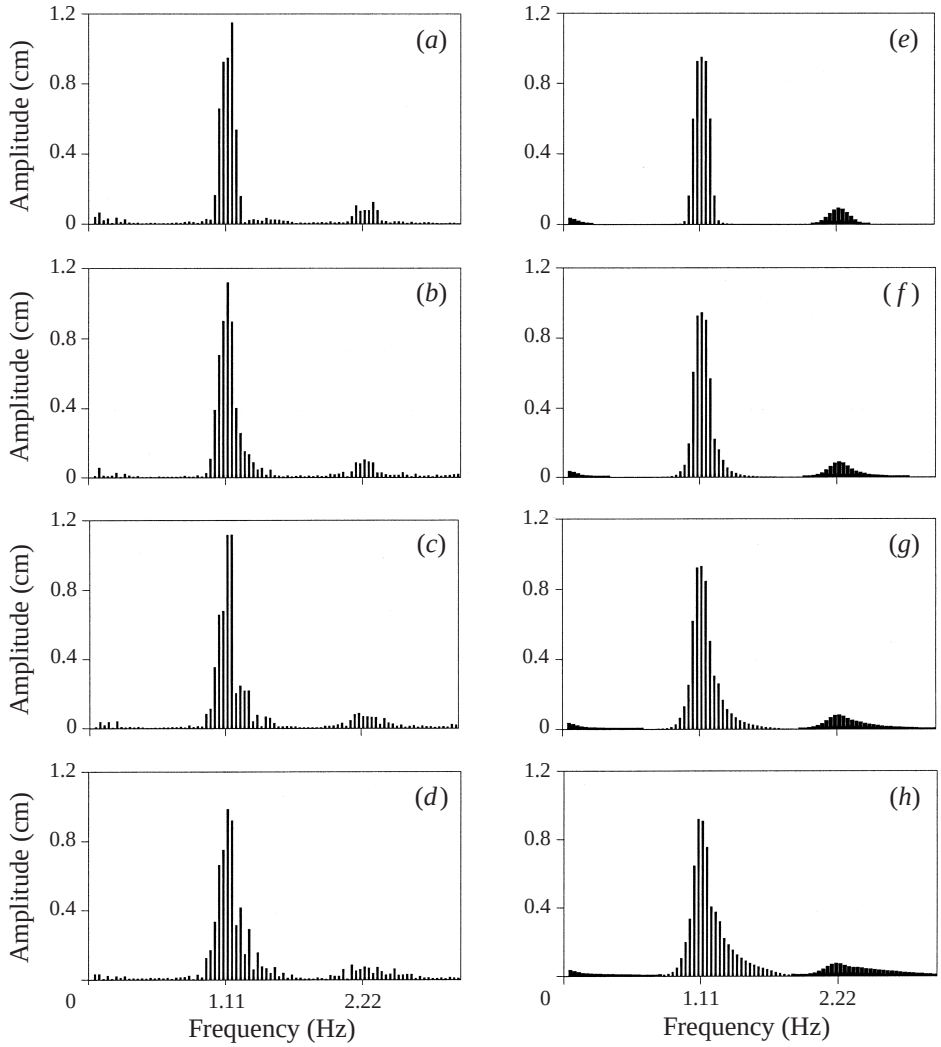

FIGURE 12. Measured (left-hand column) and simulated using 39 free modes (right-hand column) amplitude spectra. Driving signal (20), $h = 0.6$ m, $T_0 = 0.9$ s, $\varepsilon = 0.21$. Locations as in figure 7.

that the spatial Zakharov equation (17) adequately describes the evolution of the nonlinear waves along the tank at least as long as the wave steepness does not exceed $\varepsilon = 0.21$.

The effect of the wave steepness is studied in figures 12 and 13. Here $T_0 = 0.9$ s, water depth $h = 0.6$ m, so that $k_0 h = 3.0$. Wave amplitude spectra are presented in these figures for two values of the carrier wave steepness, $\varepsilon = 0.21$ and $\varepsilon = 0.14$, respectively. The agreement between the experiments and the simulations is good for both amplitudes. The spectrum widening and asymmetry are much more pronounced at the high amplitude in figure 12 than at the lower amplitude in figure 13. In fact, the amplitude spectrum in figure 13 undergoes only minor modification along the whole tank. For that reason, no other results for $\varepsilon = 0.14$, as well as for even lower amplitude, $\varepsilon = 0.07$, which were accumulated in the course of the present study, are given here.

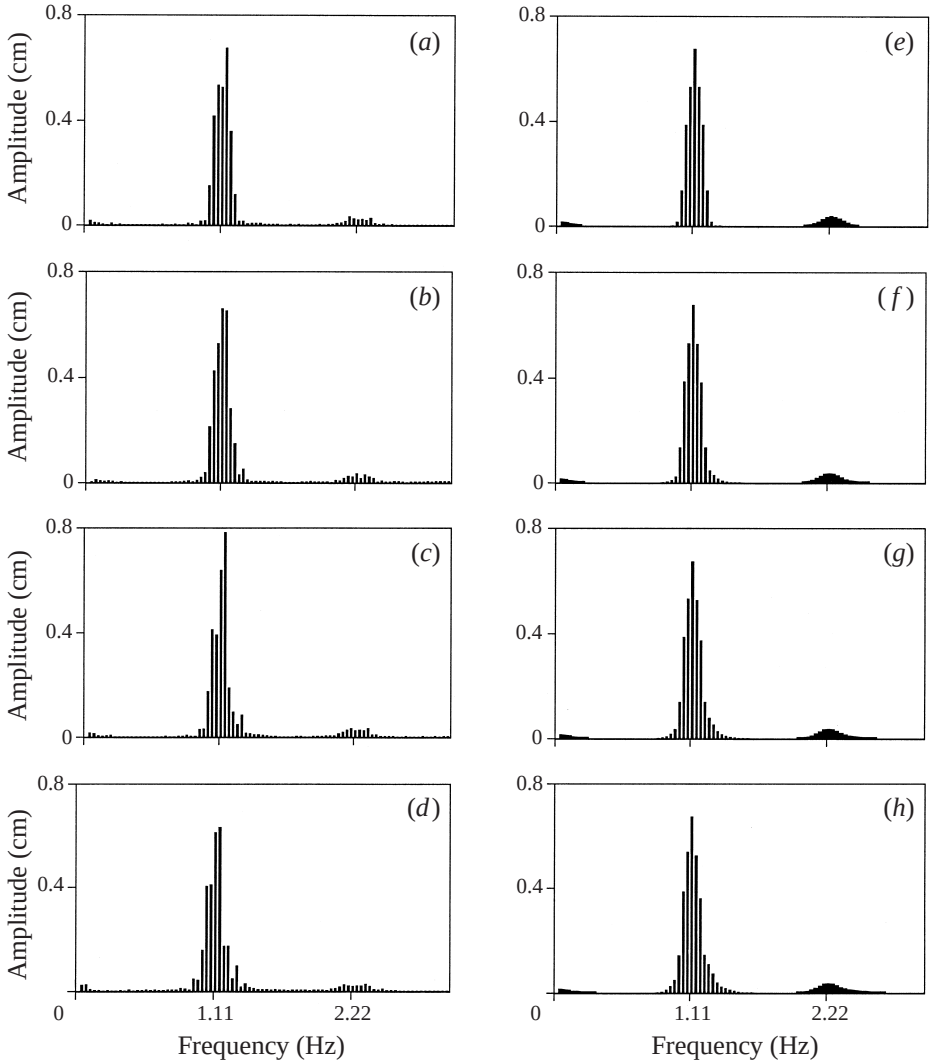

FIGURE 13. As in figure 12, except $\varepsilon = 0.14$.

The dimensionless water depths for the carrier wave frequencies in the cases considered above correspond to nearly deep-water conditions. The spatial Zakharov equation (17) is supposed to be valid for water of intermediate depth (as long as the dispersion remains sufficiently strong). Experiments and model simulations with the driving signal given by (19) at high amplitude of forcing $\varepsilon = 0.21$ were therefore performed for $T_0 = 0.7\,\mathrm{s}$ and water depth $h = 0.17\,\mathrm{m}$, so that $k_0 h = 1.54$. The agreement between the measured and the simulated amplitude spectra in figure 14 is somewhat less impressive than in the deeper water cases, in particular, with respect to the higher harmonics in the spectrum. The stimulated temporal variation of the surface elevation in figure 15, however, retains strong similarity to the experimental results. Thus, (17) still retains its validity even when dispersion becomes relatively weak.

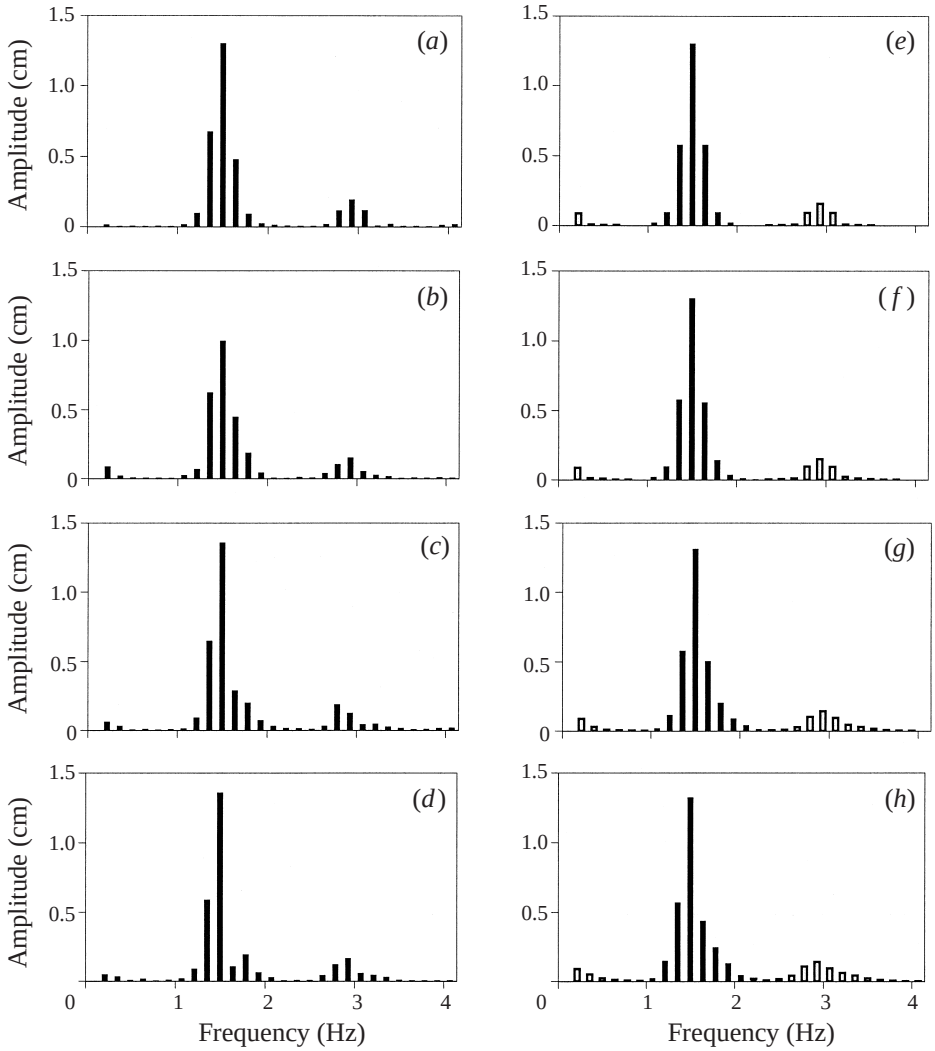

FIGURE 14. Measured and simulated (12 free modes) spectra in intermediate water depth. Driving signal (19), $h = 0.17$ m, $T_0 = 0.7$ s, $\varepsilon = 0.21$. Locations as in figure 10.

4.3. *Phase behaviour*

The spatial Zakharov model equation applied here describes the evolution of the complex wave-amplitude spectrum along the tank. The wave-amplitude spectra presented in the previous section lead to an understanding of the interaction between various modes, the mechanism of generation of new free waves and the corresponding process of the spectrum broadening. Nevertheless, the phase information in the complex wave spectra is essential in determining the eventual shape of the surface elevation variation. In this respect, figures 5(*b*) and 5(*f*) can be compared with figures 8(*d*) and 8(*h*), respectively. The driving signals in those two figures, (18) and (19), have totally different spectral shapes. The amplitude spectra obtained for these different driving signals at the remote location, however, are somewhat similar, with a single dominant peak. In spite of that, the corresponding surface elevations in figures 7(*d*, *h*) and 9(*d*, *h*) are totally different. For the bimodal initial spectrum, figure 7, each wave

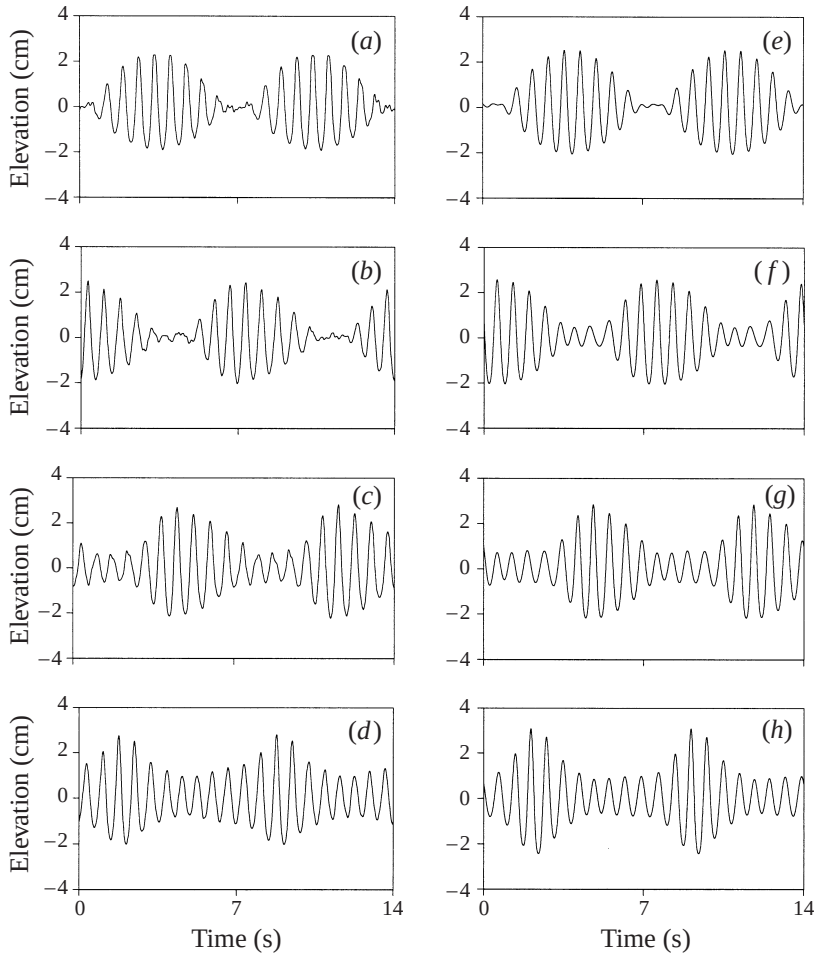

FIGURE 15. Measured and simulated surface elevations for conditions and locations of figure 14.

group retains its clear identity and the surface elevation at the boundary between the neighbouring groups remains zero. Contrary to that, no clear distinction between the groups can be seen in figure 9.

The variations of phases along the tank, computed for the four dominant modes around the carrier wave frequency are presented in figures 16(*a*) and 16(*b*) for the conditions of figure 5 and figure 8, respectively. It is obvious that the phase differences between the dominant modes behave in a different fashion in figures 16(*a*) and 16(*b*), thus contributing significantly to various surface elevation variation patterns.

5. Concluding remarks

In the present study, the experiments and the numerical simulations are carried out in an interrelated fashion in order to study the evolution patterns of nonlinear wave fields in a laboratory wave tank.

The theoretical simulations are based on the Zakharov model, in which no constraint is imposed on the frequency bandwidth. For that reason, the present simulations yield much better agreement with the experiments than the previously used

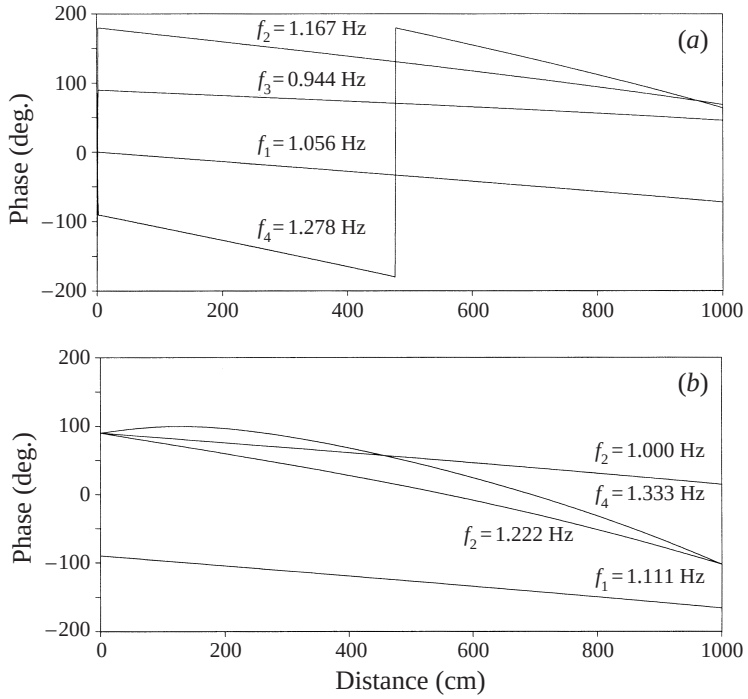

FIGURE 16. Phase variation along the tank for 4 dominant spectral components, $h = 0.6$ m, $T_0 = 0.9$ m, $\varepsilon = 0.21$. (*a*) Driving signal (18); (*b*) driving signal (19).

cubic Schrödinger model. The Zakharov model is modified here in order to describe the spatial evolution of a complicated gravity wave field in a tank.

Wave fields with three different initial spectra were considered, starting from a simple spectrum containing just two free waves, up to a fairly complicated spectrum with numerous harmonics of Gaussian shape. Values of the maximum wave steepness up to $\varepsilon = 0.21$ were considered. A procedure is developed to determine the necessary number of free waves to be considered in the model, depending on the initial spectral shape, wave amplitudes and evolution distance. Bound waves corresponding to the free wave field considered are computed and shown to contribute significantly to the temporal variation of the surface elevation in the tank.

Convincing agreement between the simulations and the experimental results is obtained. For all experimental conditions, the simulations reflected correctly the broadening of the spectrum along the tank, as observed in the experiments. Qualitative and quantitative agreement between the measured and simulated amplitude spectra was obtained at different locations along the tank. Temporal variation of the surface elevation was reconstructed from the computed complex amplitude spectra and compared with the direct wave gauge measurements at the corresponding measuring stations. In particular, impressive correspondence was obtained between the skewed wave group shapes at relatively remote locations in the experiments and the numerical simulations.

The total body of experimental and numerical results accumulated in the present study indicates that the Zakharov model constitutes an adequate theoretical model for studying the evolution of nonlinear gravity waves over intermediate and nearly deep water.

This work was supported in part by grants from Israeli Science Foundation and from INTAS.

Appendix

The jth equation describing the spatial evolution of complex amplitude $A_j = A(\omega_j, x)$ of each one of N free waves can be written as

$$c_{g_l}\mathrm{i}\frac{\mathrm{d}A_j}{\mathrm{d}x} = T_{j,j,j,j}|A_j|^2A_j + \sum_{l\neq j} 2T_{j,l,j,l}|A_l|^2A_j + \sum_{\substack{p,q\neq j \\ 2\omega_j=\omega_p+\omega_q}} T_{j,j,p,q}A_j^*A_pA_q \exp\left[-\mathrm{i}(2k_j - k_p - k_q)x\right] + \sum_{\substack{l,p,q\neq j \\ \omega_j+\omega_l=\omega_p+\omega_q}} T_{j,l,p,q}A_l^*A_pA_q \exp\left[-\mathrm{i}(k_j + k_l - k_p - k_q)x\right] \quad \text{(A 1)}$$

where $l, p, q = 1, 2, \ldots, N$.

REFERENCES

Agnon, Y. 1999 Linear and nonlinear refraction and Bragg scattering of water waves. *Phys. Rev.* E **59** (2), 1319–1322.

Agnon, Y. & Sheremet, A. 1997 Stochastic nonlinear shoaling of directional spectra. *J. Fluid Mech.* **345**, 79–99.

Benjamin, T. B. & Feir, J. E. 1967 The disintegration of wave trains on deep water. *J. Fluid Mech.* **27**, 417–430.

Dysthe, K. B. 1979 Note on a modification to the nonlinear Schrödinger equation for application to deep water waves. *Proc. R. Soc. Lond.* A **369**, 105–114.

Glozman, M., Agnon, Y. & Stiassnie, M. 1993 High order formulation of the water-wave problem. *Physica* D **66**, 347–367.

Hasimoto, H. & Ono, H. 1972 Nonlinear modulation of gravity wave. *J. Phys. Soc. Japan* **33**, 805–811.

Jiao, H.-Y. 1999 Experimental measurements and numerical simulations of nonlinear water-wave groups. PhD thesis, Tel-Aviv University.

Kit, E., Shemer, L., Pelinovsky, E., Talipova, T., Eitan, O. & Jiao, H.-Y. 2000 Nonlinear wave group evolution in shallow water. *J. Waterway, Port, Coast. Ocean Engng* **126**, 221–228.

Krasitskii, V. P. 1990 Canonical transformation in a theory of weakly nonlinear waves with a nondecay dispersion law. *Sov. Phys. JETP* **71**(5), 921–927.

Krasitskii, V. P. 1994 On the reduced equations in the Hamiltonian theory of weakly nonlinear surface waves. *J. Fluid Mech.* **272**, 1–20.

Lo, E. & Mei, C. C. 1985 A numerical study of water-wave modulation based on a higher-order nonlinear Schrödinger equation. *J. Fluid Mech.* **150**, 395–416.

Longuet–Higgins, M. S. 1978 The instabilities of gravity waves of finite amplitude in deep water. II. Subharmonics. *Proc. R. Soc. Lond.* A **360**, 489–505.

McLean, J. W. 1982 Instabilities of finite amplitude water waves. *J. Fluid Mech.* **114**, 331–341.

McLean, J. W., Ma, Y. C., Martin, D. U., Saffman, P. G. & Yuen, H. C. 1981 A new type of three-dimensional instability of finite amplitude gravity waves. *Phys. Rev. Lett.* **46**, 817–820.

Mei, C. C. 1989 *The Applied Dynamics of Ocean Surface Waves*. World Scientific, Singapore.

Melville, W. K. & Rapp, R. J. 1988 The surface velocity field in steep and breaking waves. *J. Fluid Mech.* **189**, 1–22.

Rasmussen, J. H. & Stiassnie, M. 1999 Discretization of Zakharov's equation. *Eur. J. Mech.* B *Fluids* **18**, 353–364.

Shemer, L. & Chamesse, M. 1999 Experiments on nonlinear gravity–capillary waves. *J. Fluid Mech.* **380**, 205–232.

Shemer, L., Kit, E., Jiao, H.-Y. & Eitan, O. 1998 Experiments on nonlinear wave groups in intermediate water depth. *J. Waterway, Port, Coast. Ocean Engng* **124**, 320–327.

Shemer, L. & Stiassnie, M. 1985 Initial instability and long-time evolution of Stokes waves. In *The Ocean Surface: Wave Breaking, Turbulent Mixing and Radio Probing* (ed. Y. Toba & H. Mitsuyasu), pp. 51–57. D. Reidel.

Shrira, V. I., Badulin, S. I. & Kharif, C. 1996 A model of water wave 'horse-shoe' patterns. *J. Fluid Mech.* **318**, 375–404.

Stiassnie, M. 1984 Note on the modified Schrödinger equation for deep water waves. *Wave Motion* **6**, 431–433.

Stiassnie, M. & Shemer, L. 1984 On modifications of the Zakharov equation for surface gravity waves. *J. Fluid Mech.* **143**, 47–67.

Stiassnie, M. & Shemer, L. 1987 Energy computations for evolution of class I and II instabilities of Stokes waves. *J. Fluid Mech.* **174**, 299–312.

Su, M. Y. 1982 Three-dimensional deep-water waves. Part 1. Experimental measurements of skew and symmetric wave patterns. *J. Fluid Mech.* **124**, 73–108.

Trulsen, K. & Dysthe, K. B. 1997 Frequency downshift in three-dimensional wave trains in a deep basin. *J. Fluid Mech.* **352**, 359–373.

Yuen, H. C. & Lake, B. M. 1975 Nonlinear deep water waves: theory and experiment. *Phys. Fluids* **18**, 956–960.

Yuen, H. C. & Lake, B. M. 1982 Nonlinear dynamics of deep-water gravity waves. *Adv. Appl. Mech.* **22**, 67–229.

Zakharov, V. E. 1968 Stability of periodic waves of finite amplitude on the surface of a deep fluid. *J. Appl. Mech. Tech. Phys.* **9**, 190–194.